

Electro-thermal quench in metal-insulated nested REBCO coils for magnets over 40 T

Anang Dadhich¹, Philippe Fazilleau² and Enric Pardo^{1*}

¹Institute of Electrical Engineering, Slovak Academy of Sciences,
Bratislava, Slovakia

²Université Paris-Saclay, CEA, Département des Accélérateurs,
de la Cryogénie et du Magnétisme, 91191, Gif-sur-Yvette, France

*Author to whom correspondence should be addressed
(enric.pardo@savba.sk)

February 16, 2026

Abstract

Superconducting high field magnets have the capability to generate over 40 T, with multiple existing practical applications globally. However, at such high magnetic fields, these magnets are prone to rapid electrothermal quench which can affect the continuous operation of such magnets. A nested stack configuration, with multiple HTS inserts inside a LTS outer-sert, can be used for better thermal stability and compact design. We have performed detailed multiphysics quench analysis of such a nested stack high field magnet design under SuperEMFL project using our in-house software, which considers screening currents. Through various case studies, we have identified various weak spots in such a magnet, where thermal quench can be the most detrimental for magnet operation, and various ways are suggested to overcome this important issue.

1 Introduction

Coils made of REBCO High Temperature Superconductors (HTS) can generate high magnetic fields thanks to their high engineering current density. Thus, REBCO coils have many interesting applications in high field magnets [1–6, 6–11], medical research [12–15], fusion [16, 17], aircraft electric propulsion [18–24], space electric propulsion [25, 26], and other rotating machines [27–29]. For high field magnets, pancake HTS coils are used, and these magnets are able to generate over 30-40 T magnetic field [5, 30, 31]. For example, the Nougat

project's HTS magnet (insert) was designed to generate 10 T, and inserted in a 20 T resistive magnet outsert, to give a combined 30 T field [32]. Using metal insulated winding at 4.2 K, the Nougat magnet measured up to 32.5 T [4]. For SuperEMFL project, which intends to use a Low Temperature Superconductor (LTS) outsert instead of resistive magnet with an HTS insert, we aim to generate 32 T and 40 T, through different designs [5, 6, 30, 31, 33]. Globally, other high field magnets are also able to generate fields in this range, or are currently under development, such as the LBC hybrid demonstrator magnet (45.5 T) in Florida, USA [1,34], CHFML hybrid magnet (45 T) in Hefei, China [10], HFLSM magnet (25-30 T) in Tohoku, Japan [7,35], Grenoble hybrid LTS magnet in France (43 T) [36], among other.

Along with the aforementioned benefits, superconducting high field magnets also present many challenges. Firstly, superconductors are diamagnetic materials, which present magnetization and screening currents. These generate high AC losses during the ramping up of the magnet [31, 33, 37]. Furthermore, when the current in the magnet goes over the critical current (I_c) of the HTS, resistive heat is generated, which can lead to thermal runaway or 'quench', that risks the burning of the material if not controlled. Localized damage or inhomogeneity of material can also cause thermal hotspots, leading to quench [38–42]. Therefore, a high field magnet design needs to be thermally sound, with fail-safe techniques like voltage limiting, which can work for high field magnets using non-insulated or metal insulated windings [42]. Adding an insert to high field outsert magnet tackles many of these issues, such as better thermal management (for instance, LTS outsert and HTS insert can have their own cooling media and cryogenic systems), scalability and ease of repair (coils can be replaced much easily in the case of damage and upgrade), improving the mechanical strength, and developing a compact design to generate high magnetic fields at the center of magnet as compared to single pancake stacks or solenoids [43–45]. This design can be further improved by inserting multiple HTS stacks ('or nested stacks') in LTS outsert to give better thermal stability (different inner stacks quench at different times, and can be thermally managed better) [5] and mechanical strength (as the multiple pancake coils can share the less turns, i.e. less stress accumulation). A multiple nested inner stack system, with 3 nested HTS coils, was tested recently at MIT for NMR magnets, and serves as a good demonstrator for this technology [46].

Also, as we see that the design of high field magnets involves complex and coupled multiphysics, a strong and fast software is required in the superconducting community to analyze these cases, as the commercial software can be very limited and slow in simulating these issues [31]. This is mainly because of the high number of pancake coils in the system (at least 15), and each consisting of 200 or more turns. Furthermore, most electrothermal quench models consider uniform current density in HTS tapes due to ease of modeling and fast computation times [39, 47–50], but that misses out on additional AC losses generated by screening currents, which contribute significantly to the temperature rise in such high field magnets [31, 42].

A nested stack system is currently being designed under SuperEMFL project,

which involves 2 HTS nested stack insert inside a LTS stack outsert, and can generate higher fields at center (up to 45 T) as compared to normal solenoid designs [5]. This paper is focused on detailed multiphysics analysis (electrothermal and electromagnetic) of this nested stack system, using our in-house software that considers screening currents. Under this analysis, we have focused on thermal quench of the HTS inserts under different damage circumstances. Voltage limiting features are also applied to the design in the event of quench, to control the thermal runaway and letting the magnet to operate at lower power output. Doing so, we have identified various thermally weak points in such high field nested stack systems from where electrothermal quench can be detrimental to magnet operation.

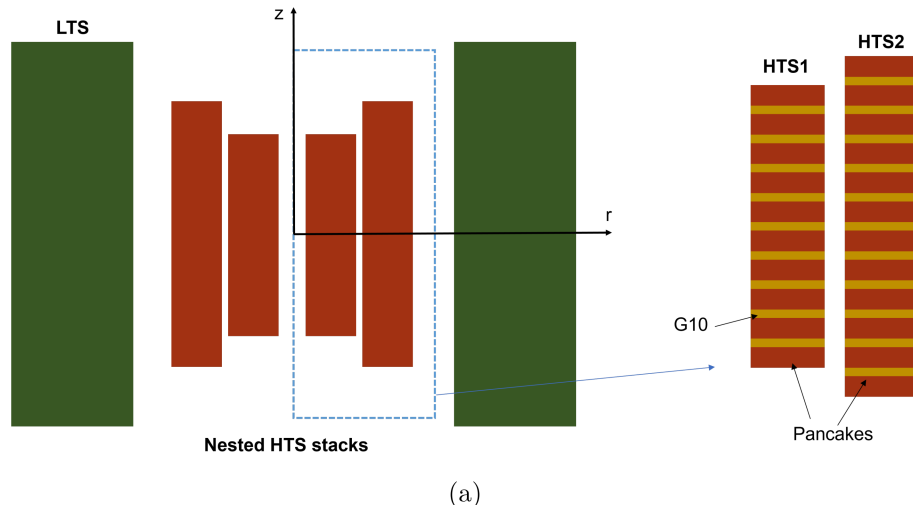
2 Modeling Method

An in-house 2D axi-symmetric software is used to calculate different cases for this paper. The electromagnetic calculations are performed by the Minimum Electro-Magnetic Entropy Production (MEMEP) method, which is based on variational principles [33, 51, 52]. This method takes both screening currents and radial currents into account. The thermal calculations are performed using explicit Finite Difference (FD) method. MEMEP and FD are coupled together to give accurate results (MEMEP-FD). This method considers temperature dependent electromagnetic and thermal properties, and this coupling is shown in our previous works [31]. These methods have been also benchmarked for pancake and racetrack coils with various mainstream methods and commercial software based on Finite Element Method to prove its validity [53, 54]. Additionally, voltage limiting features are added as a fail-safe method to limit the current input in the case of quench [42]. Each simulation for this paper took around 3 days to complete in a standard desktop computer, which is fast considering the high number of pancakes and turns per pancake in the nested stack system (parameters described in Table 1).

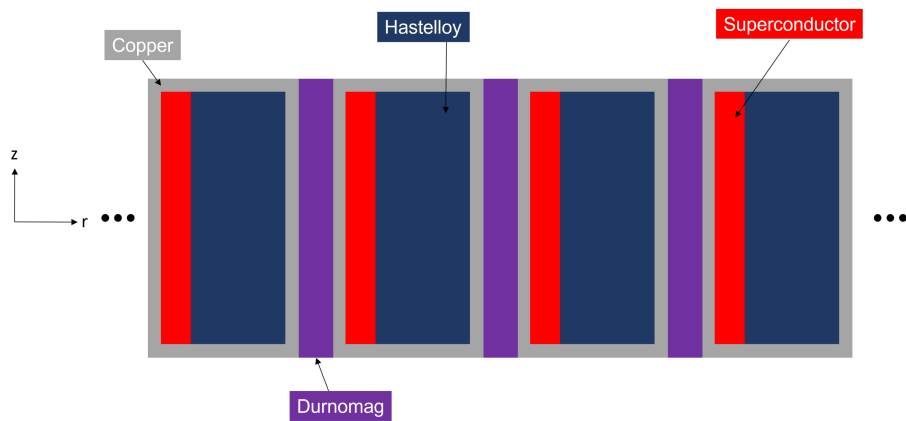
3 Modeling parameters

We consider a user magnet design from the SuperEMFL project (basic design N1 for the 40 T magnet) [5]. The LTS outsert is a 15 T/250 mm bore magnet from Oxford Instruments [30]. These summarized parameters are shown in Table 1. The complete magnet system consists of LTS outsert, and an HTS insert made of two nested stacks of metal-insulated pancake coils with their own power (electrical) circuit, as shown in Figure 1(a). The HTS1 stack is connected to the HTS2 stack in series, and the LTS stack provides a background field of around 15 T to the nested HTS stacks. This whole system is initialized at 4.2 K, i.e. liquid Helium temperature.

For the calculations, Theva APC tape is considered (APC stands for Advanced Pinning Center), and its dimensions are given in Table 1. The cross



(a)



(b)

Figure 1: (a) Full scale magnet and its cross section, which shows nested HTS1 and HTS2 pancake coil insert stacks inside LTS outsert magnet. (b) Cross section of turns in pancakes, including the isolating Durnomag layer between 2 tapes. The sketches are only for representation and not to scale.

Table 1: Design parameters of the HTS metal-insulated nested stack [5]. Copper thickness refers to the total thickness across the tape.

Nested stack dimension	Values	Material dimensions	Values
Internal Diameter	50 mm	REBCO	2 μm
External Diameter	216.2 mm	Substrate (Hastelloy)	54 μm
HTS1 pancakes	42	Copper	10 μm
HTS2 pancakes	44	Durnomag	30 μm
HTS1 turns per pancake	360	G10 width	0.5 mm
HTS2 turns per pancake	260	Pancake/tape width	6 mm
LTS magnetic field	15 T	Durnomag resistivity	$10^{-6} \Omega\cdot\text{m}^2$
Limiting voltage	2.5 V	Nominal current	231.2 A

section in the thickness of the tape is shown in Figure 1 (b). The temperature and magnetic field dependent electromagnetic and thermal properties of the tape layers, including the tape design and assumptions can be seen in our previous works [31, 42]. Neighboring turns are separated by a metal layer of Durnomag, which allows for radial currents between layers. A complete $J_c(B, T, \theta)$ dependence of Theva tape is considered for calculations [42, 55], which allows to consider the decrease in the localized current density with magnetic field and temperature.

We analyze quench due to a group of damaged turns. As a worst-case scenario, we consider that J_c drops to 10 % of its original value in the damaged turns. The damaged group of turns is 41 to 50 turns (10 turns in total), and the specific pancake where the damage occurs is specified in the next sections, case wise. The reason for using 10 turns as a group, is due to the homogenization of 10 turns as one homogenized block in our simulations to improve the speed of the calculations [33]. The magnet is set to be running at a steady nominal current (231.2 A) as an initial condition, when damage appears. Hence, the quench is analyzed from this point in time, with a fixed time step of 10 milliseconds. These studies also assume adiabatic conditions at the boundary of the nested stacks, i.e. no heat is exchanged with the external coolant or extracted from the system. Lastly, the turn-to-turn contact resistivity of the winding (or Durnomag layer here) is considered to be $10^{-6} \Omega\text{m}^2$ (typical of metal insulated windings [56]) in all cases, unless specified.

Additionally, HTS1 and HTS2 are thermally and electrically isolated from each other, and hence they interact only through inductive effects. The current density and temperature profiles shown in the next section are for the cross section as shown in Figure 1 (a).

4 Results and Discussion

The electrothermal quench in the HTS nested stacks is studied in the next sections, for different case scenarios and parameters. Firstly, we study the effect of the location of the damage (weak spot) in the inner HTS stack. All these studies are performed considering the screening currents distribution in the simulations.

This is a key feature for quench analysis, since assuming uniform current density under-estimates electrothermal quench propagation speed [42]. Thus, a case with uniform current density (J) has been added in the 1st study to show the impact of screening currents for nested stacks. Secondly, we make a parametric study of the contact resistance between turns. Lastly, we analyze the effect of damage at the outer stack (HTS2).

4.1 Study 1: Weak spot location

This section analyses the impact of the weak spot location in the nested stack configuration. For this purpose, damage is induced in 10 aforementioned turns in different pancakes in the inner stack (HTS1): top, bottom, and middle pancake. The results for this study is shown in figures 2-5.

Figures 2-4 show azimuthal current density, change in temperature ($\Delta T = T - T_{\text{initial}}$, where $T_{\text{initial}} = 4.2$ K), and radial current profiles when the damaged turns are at the top, middle, and bottom pancakes of the HTS1 stack, respectively. At each turn, the total current is the azimuthal current plus the radial current. Then, the coil total current consists on the average azimuthal current plus the average radial current in the coil cross-section. The following general behavior for these stacks can be seen from these profiles: the change in temperature is the highest in the damaged turns, which decreases the azimuthal current density in these turns and gives rise to the radial currents. This temperature rise propagates through the whole HTS1 stack, decreasing the critical current density everywhere (or transiting the superconductor to normal state ($T > T_c$)). As a consequence, radial currents rise. These radial currents further increase the power losses and temperature of the magnet, as we have seen in our previous work [31]. Thus, quench occurs in the whole stack quickly due to this quench propagation. Another major reason for such high power losses is the presence of screening currents in the system, which gives rise to high AC losses [42]. The swift changes in magnetic field from the HTS1 stack also affect the HTS2 inductively that contributes to its quenching, and it can be seen from these figures that both nested stacks quench almost simultaneously. Consequently, decrease in angular currents in HTS2 also contributes in inducing quench in HTS1.

These figures also show that the configuration where the damage is at the top of the HTS1 stack quenches much faster than the other 2 cases, which is around one second (see Figure 2 (a)-(c)). Comparatively, the case with the damage at bottom, takes the longest time to quench (up to 3 seconds) as seen in Figure 4 (a)-(c). However, the temperature rise is the highest in the latter case (up to 300 K, as also seen in Figure 5 (e)), as compared to the others. Then we can consider this as the worst case scenario, due to the higher chances that the HTS tape can experience damage by electro-thermal mechanical stress. Thus, the next studies in this paper considers damage at the bottom of HTS1 as the reference case for detailed calculations.

The reason for the faster quench in the bottom damaged case is the $J_c(B, T, \theta)$ behavior of the considered Theva HTS tape. The angular dependence of J_c is

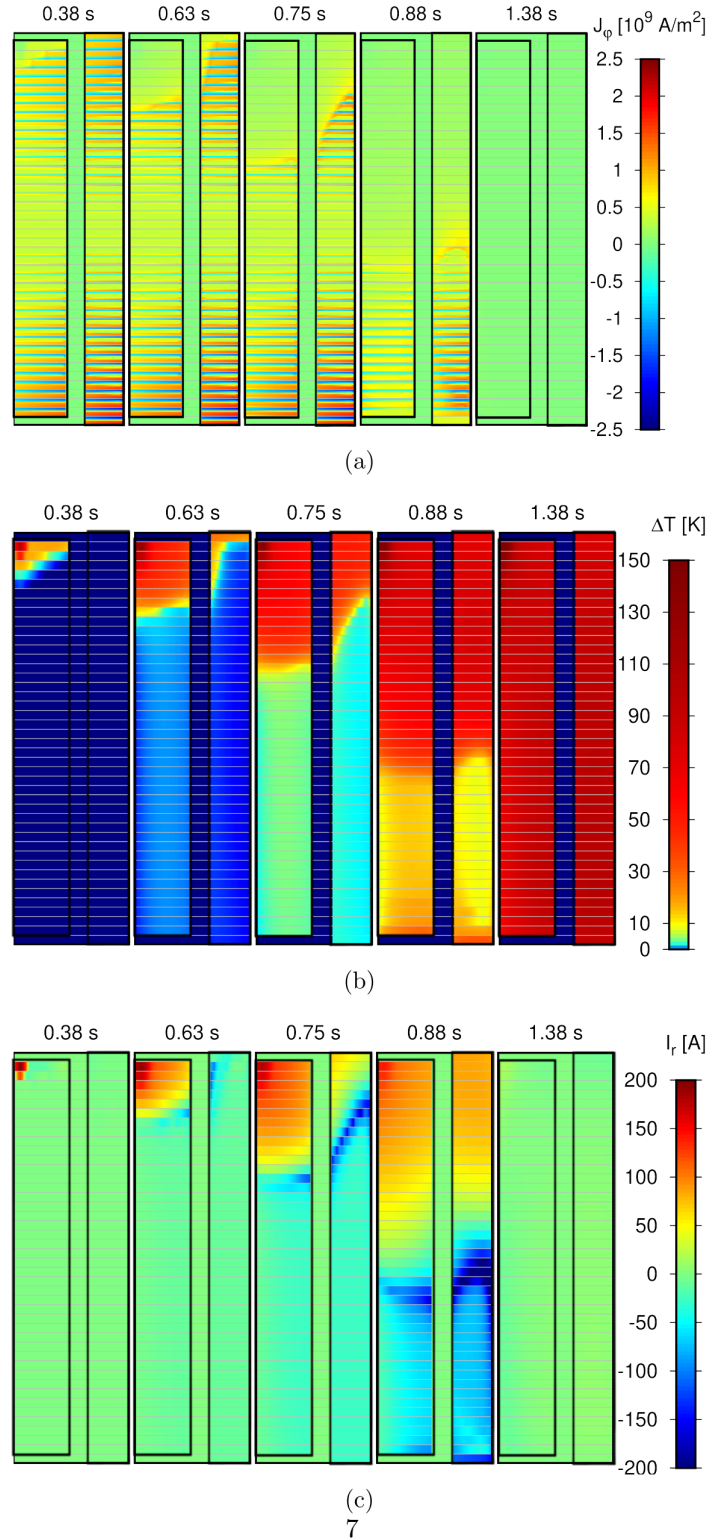


Figure 2: Hotspot analysis when damage is at the top pancake at HTS1. Figure shows (a) current density profiles, (b) change in temperature, and (c) increase in radial currents up to 1.38 s.

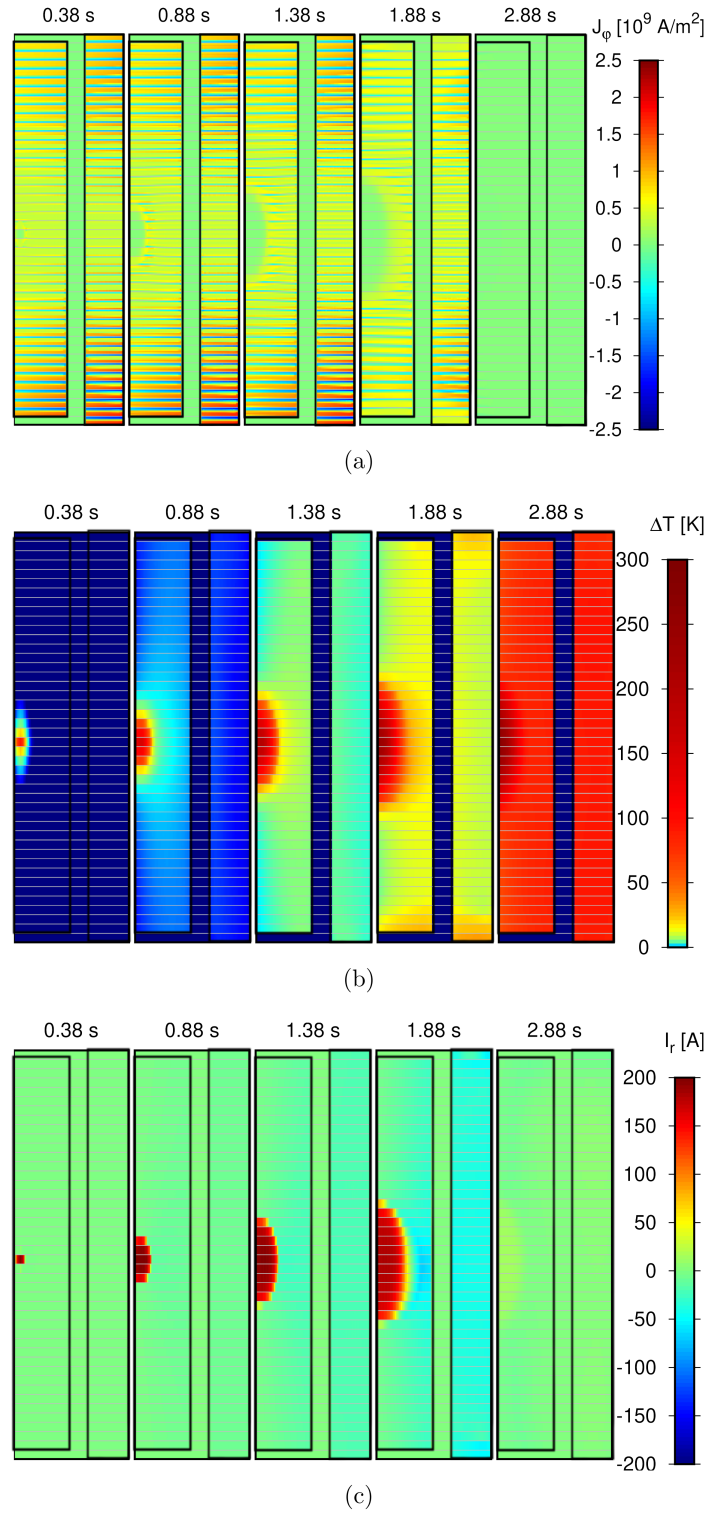


Figure 3: Hotspot analysis when damage is at the middle pancake at HTS1. Figure shows (a) current density profiles, (b) change in temperature, and (c) increase in radial currents up to 2.88 s.

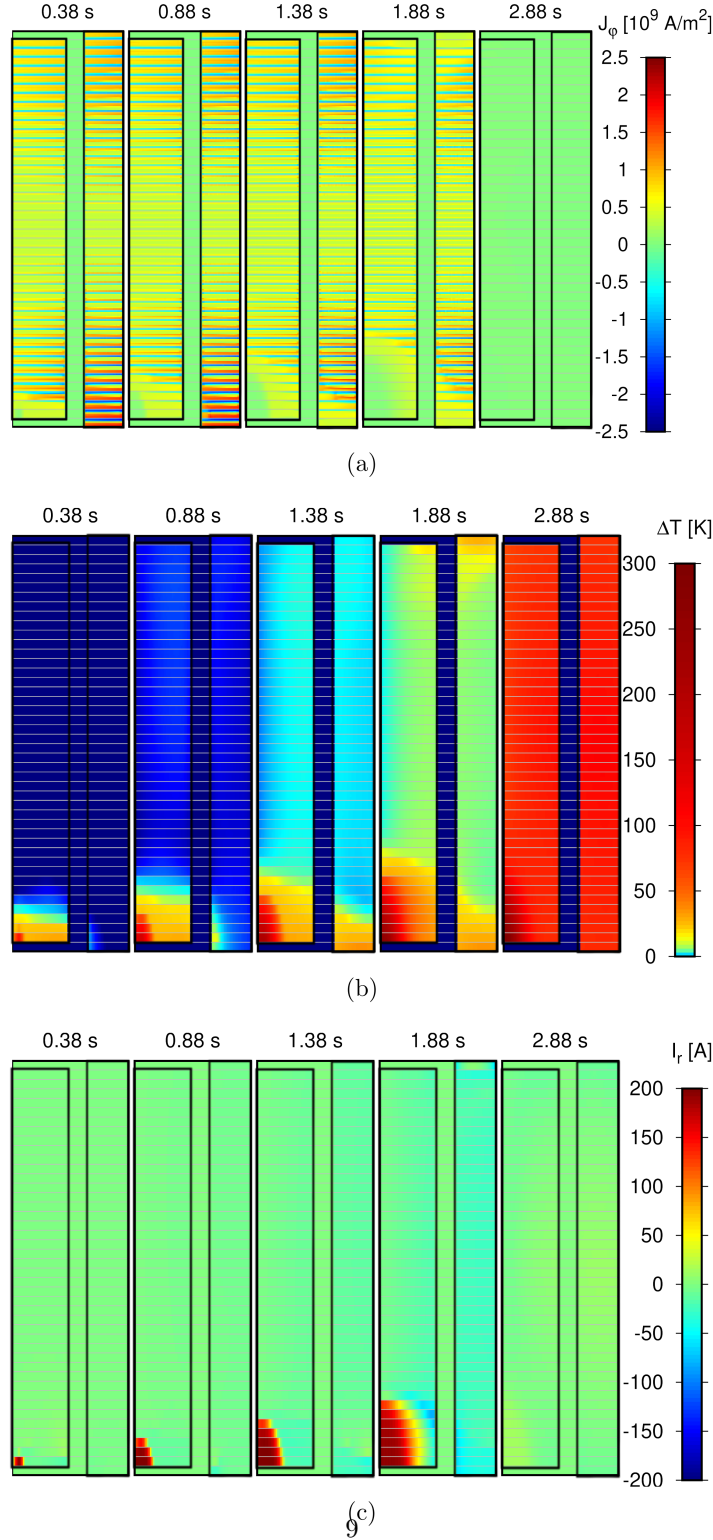


Figure 4: Hotspot analysis when damage is at the bottom pancake at HTS1. Figure shows (a) current density profiles, (b) change in temperature, and (c) increase in radial currents up to 2.88 s.

non symmetric with respect to the tape plane, with angular deviation around 30° , and varies highly around the 90 degree field angles [42], which makes its J_c much lower at the top of the nested stack as compared to the bottom. Due to this lower J_c at the top, the nested stack quenches much faster at the top, while the quench also propagates faster. At the bottom, J_c is higher, which keeps most of the pancakes superconducting. However, then the quench propagation is also slower which keeps the heat accumulated in the smaller damaged sections and it gives rise to higher maximum temperature. Other REBCO tapes, like Fujikura, do not have this asymmetry, and quench may propagate more symmetrically from both top and bottom [31, 42].

Figure 5 shows several electrical and thermal quantities of the complete nested stack. Firstly, Fig. 5 (a) shows a drop in the total current due to voltage limitation and the appearance of non-superconducting parts due to electrothermal quench (or the decrease of the I_c of several turns below the operating current). Without voltage limitation, the total power would increase monotonically, leading to thermal runaway. There is rise in total power due to the current density overcoming local J_c , which gives rise to temperature (Figures 5 (c) and (e)). This increase in temperature further reduces J_c , and hence there are more coil turns with current higher than local I_c , contributing further to the total power rise (mainly azimuthal). Also, this fast change in screening currents (azimuthal direction) causes significant AC losses [42]. The azimuthal current at each turn gets converted to radial currents during electrothermal quench; which gives rise to the radial power, or power due to radial currents (Figure 5 (d)). This radial power also contributes to the temperature rise in the magnet [31, 33]. These negative average radial currents seen in Figure 5 (b) are due to the induced effects due to the decrease in magnetic flux caused by the decrease in average angular current. Figures 5 (e,f) show that when damage appears at the bottom, electrothermal quench is the slowest but the maximum temperature is the highest. For all configurations, the average temperature overcomes the critical temperature, 92 K (Figure 5 (f)).

It is interesting to note that the case with damage at the middle of HTS1 stack shows the highest radial power and radial currents, and the maximum temperature for this case is almost the same as the reference case (Figure 5). The reasons are the following. First, the maximum temperature occurs at the damaged turns. Since their I_c is well below the operating current, their loss is dominated by the turn resistance in the angular and radial directions and the instantaneous current. As electro-thermal quench propagates at an intermediate speed between the cases of damage on top and bottom, the coil current drops at an intermediate time. Therefore, the accumulated heat in the damaged turns is in between that for damage at top and bottom. Thus, the maximum temperature for damage in the middle is in between. The highest radial power is due to the fact that, once the pancake with damage fully quenched, quench propagates both upwards and downwards, as well as radially.

We also show one case in figures 5 (a)-(f) considering uniform current density instead of screening currents in the simulation, where damage is at the top pancake in HTS1 (red dashed curve). Here, it is seen clearly that the quench

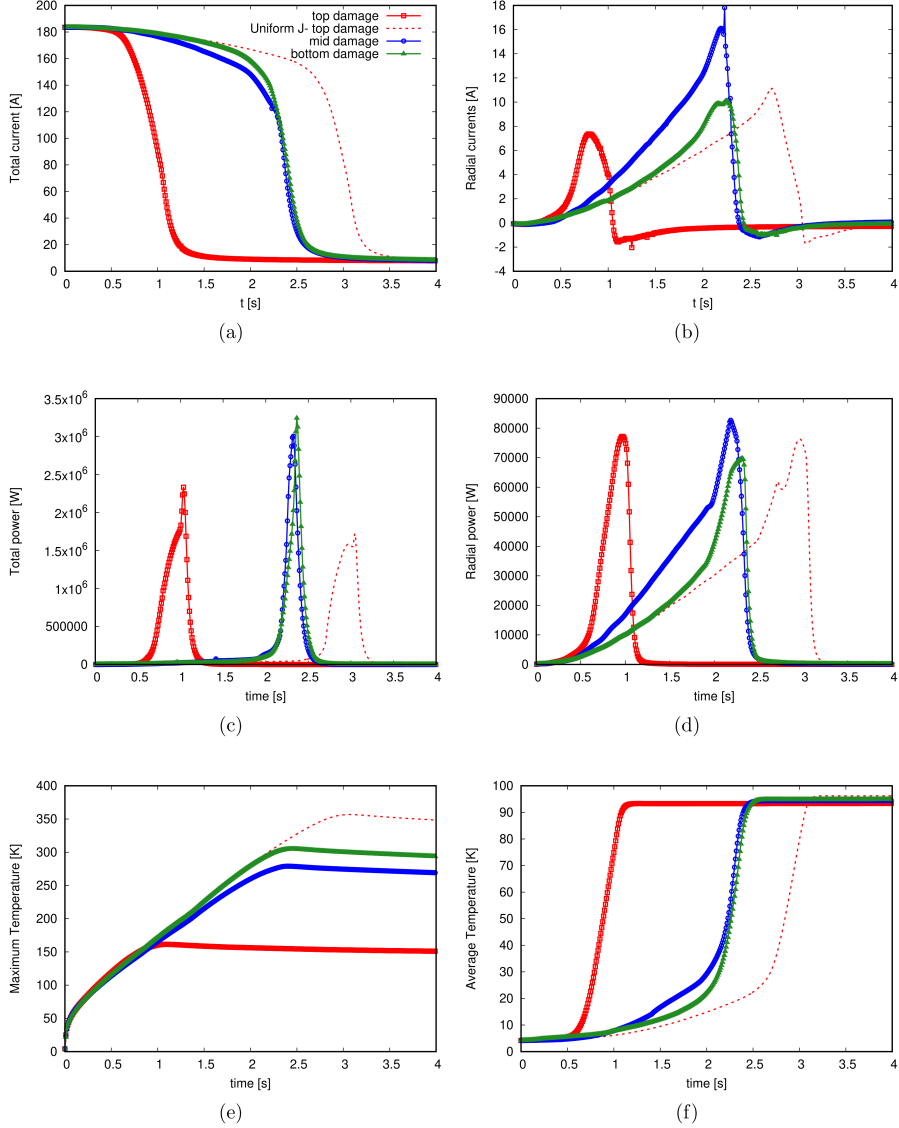


Figure 5: Nested stack behavior when damage occurs at different parts of the stack. Figures show (a) Total current decay, (b) Average radial current in section, (c) Total power, (d) Power loss due to radial current, (e) Maximum temperature, and (f) Average temperature rise in the nested stacks after the onset of damage. It is seen that maximum temperature rise occurs when the damage is at the bottom of the stack, and hence it is considered as the worst case scenario (or our reference case). All figures use same legend as (a).

predicted by such assumption is not accurate, as widespread quench appears after almost triple the time than when screening currents are present (red solid curve). It also shows the highest maximum temperature, which shows that this prediction may not be accurate, compared to when screening currents are present, which is more realistic and physical case. This is consistent with our previous work in [42].

4.2 Study 2: Effect of contact resistance between turns

Since we observed in the previous section that the quench at the bottom of HTS1 stack is potentially the most damaging, next we study the effects on such quench when varying the contact resistance between turns. The previous study was done with turn-to-turn resistivity as $10^{-6} \Omega \cdot \text{m}^2$, and in the following we also consider $10^{-7} \Omega \cdot \text{m}^2$ and $10^{-8} \Omega \cdot \text{m}^2$. The results for this study is shown in figures 6 and 7.

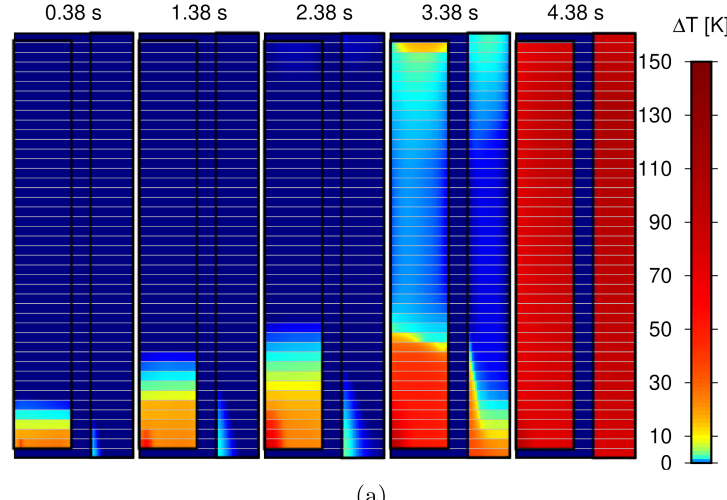
Firstly, it is seen from Figures 6 and 4(b), that the case with the highest turn-to-turn contact resistance ($10^{-6} \Omega \cdot \text{m}^2$) is the fastest to quench (in less than 3 seconds). The case with contact resistance of $10^{-7} \Omega \cdot \text{m}^2$ quenches in around 4.3 seconds, and the case with $10^{-8} \Omega \cdot \text{m}^2$ does not quench at all, even after 8 seconds (almost 4 times longer than the reference case). However, the maximum temperature increases with the contact resistance. We have seen these effects in our previous works about single-stack inserts [31, 33]. The quench in nested stacks can be further reduced by using soldered coils or joints (with resistivities equal or below $10^{-9} \Omega \cdot \text{m}^2$), as being considered for certain REBCO magnets [57, 58]. These may be complicated to build, but they are effective in avoiding delamination due to thermal stress during quench; thanks to lower thermal gradients [57–59]. Soldered coils are better regarding thermal stabilization. However, they strongly limit the ramp rate, and may not be suitable for the user magnets for the SuperEMFL project, which require relatively fast ramp rates.

Figure 7 shows further analysis for this study. It can be seen here that the non-insulated magnet shows almost no drop in the total current, or no rise in the total power, when compared to the other two metal insulated cases. The average and maximum temperature rises very slightly for the non-insulated case (Figure 7 (d) and (c)), whereas the metal-insulated magnet has already quenched within 4 seconds for both 10^{-6} and $10^{-7} \Omega \cdot \text{m}^2$.

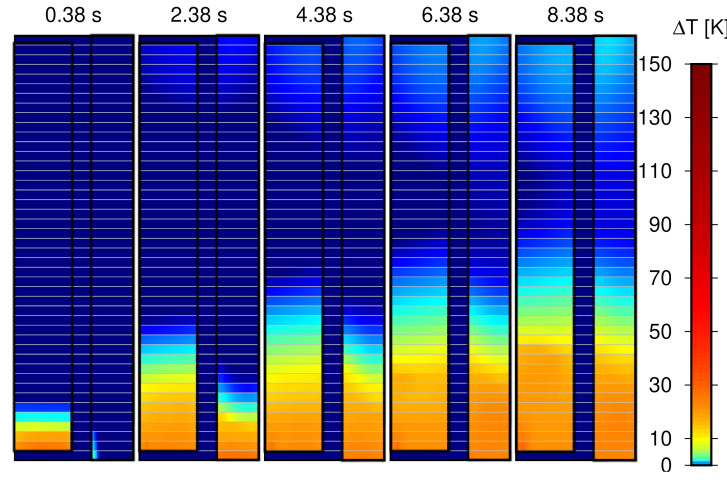
4.3 Study 3: Damage at outer stack

Lastly, we also check the effect on quench when it occurs due to damaged turns in the outer stack (HTS2). The results for this configuration is shown in figures 8 and 9. These results are compared with the reference case (damage at the bottom of HTS1).

The behavior is similar to when quench appears in the inner stack. The case with the damage at the top quenches faster (Figure 8 (a): 1.78 s) than the damage at the bottom of HTS2 stack (Figure 8 (b): 6.38 s). This consequently



(a)



(b)

Figure 6: Resistivity analysis with different turn to turn resistance. Figure shows change in temperature when turn-to-turn resistivity is (a) $10^{-7} \Omega \cdot \text{m}^2$, and (b) $10^{-8} \Omega \cdot \text{m}^2$

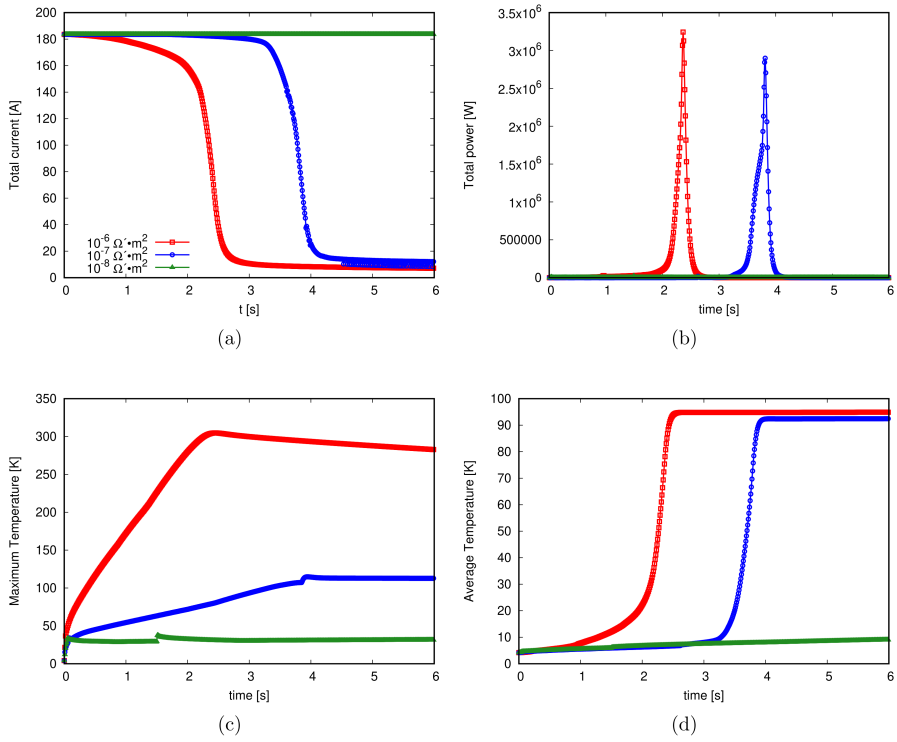
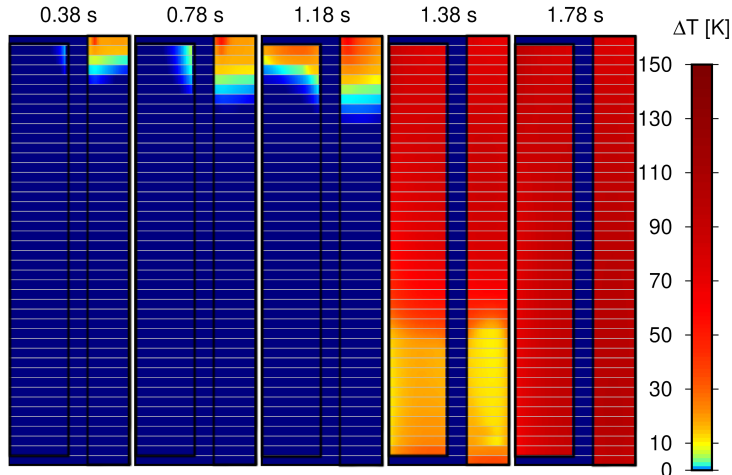
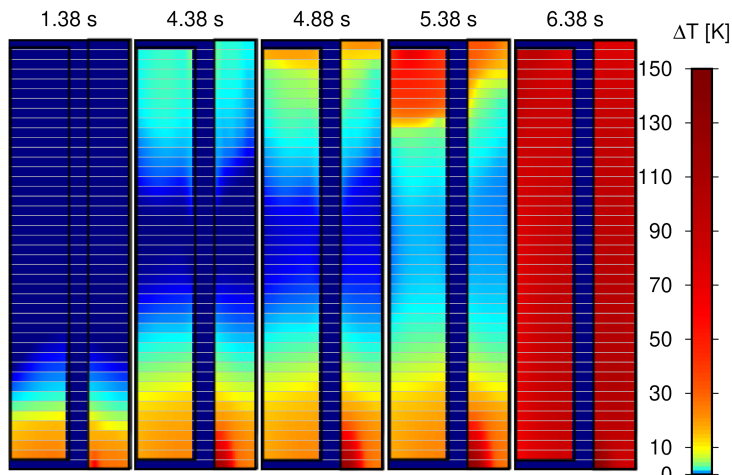


Figure 7: Resistivity analysis with different turn to turn resistance. Figures show (a) Total current decay, (b) Total power, (c) Maximum temperature, (d) Average temperature rise in nested stacks after the onset of damage. All figures use same legend as (a).



(a)



(b)

Figure 8: Nested stack behavior when damage occurs at different parts of the outer stack. Figure shows change in temperature when damage is at (a) top, and (b) bottom of HTS2 stack.

quenches the inner HTS1 stack as well, simultaneously. This is further verified from Figure 9 (f), where the average temperature of the whole insert rises above critical temperature much later for the bottom damaged HTS2 stack than any of the other cases. The reason why quench for damage at the bottom of HTS2 appears later than if quench is at HTS1 is because the magnetic field at HTS2 is lower, and hence J_c at HTS2 is higher. Therefore, the safety margin in the outer stack is higher, which causes the quench to appear later.

The maximum temperature for both cases of quench in the outer stack is quite similar, with only around 20 K difference (Figure 9 (e)), in contrast to the quench in the inner stack. The lower increase in temperature compared to the quench in the inner stack is because the radius of the damaged turns in the outer stack is higher. Then, the heat inertia is higher, and hence it requires more heat to increase the temperature. In addition, the turn-to-turn resistance decreases with the radius for the same contact resistance. Also, similar radial current and radial power rise for these 2 cases (Figure 9 (b) and (d)) contributes to the temperature rise. The reference case still shows the highest maximum temperature of around 300 K, and thus it is the most sensitive point of such a magnet design, which can quench the whole magnet with very high temperatures.

5 Conclusion

A nested stack configuration with two HTS REBCO nested stacks insert within a LTS outsert is successfully analyzed numerically for multiphysics quench, using our in-house software. It is seen that the bottom pancake of the innermost stack (HTS1) is the most sensitive to the electrothermal quench, showing the highest maximum temperature in all cases. Thus, precautionary measures should be taken to make this section thermally stable. This effect can be further reduced using lower resistivities between turns (below $10^{-7} \Omega \cdot \text{m}^2$) for successful long term operation of such high field magnets. However, lower contact resistance between turns will limit the ramp speed of high-field magnet, and hence an optimum value should be obtained for the particular use of the magnet.

6 Acknowledgements

We acknowledge Oxford Instruments for providing details on the cross-section of the LTS outsert. This work has received funding from the European Union's Horizon 2020 research and innovation programme under grant agreement No 951714 (superEMFL), and the Slovak Republic from projects APVV-24-0654 and VEGA 2/0098/24. Research partially funded by the EU NextGenerationEU through the Recovery and Resilience Plan for Slovakia under the project No. 09I04-03-V02-00039. Part of the research results were obtained using the computational resources procured in the national project National competence centre for high-performance computing (project code: 311070AKF2) funded by the European Regional Development Fund, EU Structural Funds Informatization

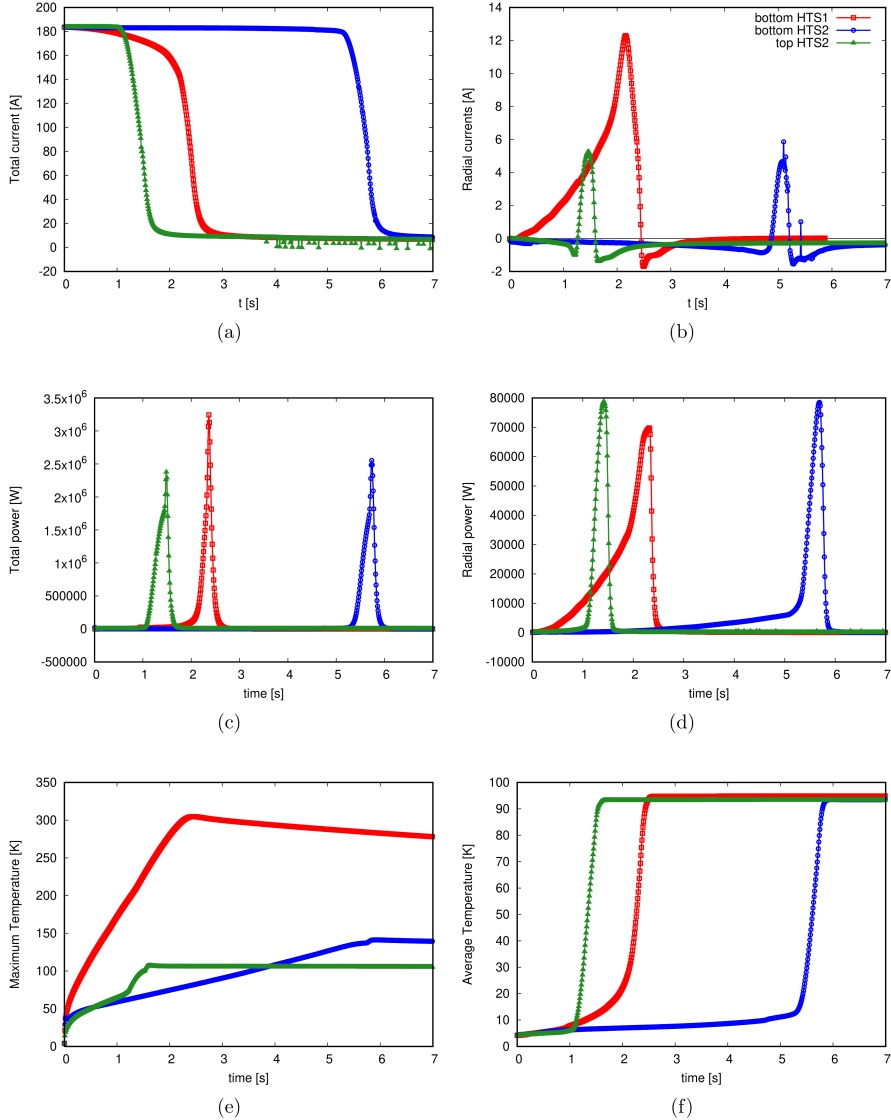


Figure 9: Nested stack behavior when damage occurs at different parts of the outer stack. Figures show (a) Total current decay, (b) Radial current rise, (c) Total power, (d) Radial power, (e) Maximum temperature, and (f) Average temperature rise in nested stack after the onset of damage. It is seen that maximum temperature rise occurs when the damage is at the bottom of the HTS1 stack, which is the weak point of the whole system. All figures use same legend as (b).

of society, Operational Program Integrated Infrastructure. Any dissemination of results reflects only the authors' view and the European Commission is not responsible for any use that may be made of the information it contains. AD acknowledges the Schwarz Fund from the Slovak Academy of Sciences.

7 References

References

- [1] Seungyong Hahn, Kwanglok Kim, Kwangmin Kim, Xinbo Hu, Thomas Painter, Iain Dixon, Seokho Kim, Kabindra R Bhattarai, So Noguchi, Jan Jaroszynski, et al. 45.5-tesla direct-current magnetic field generated with a high-temperature superconducting magnet. *Nature*, 570(7762):496–499, 2019.
- [2] Hongyu Bai, Mark D Bird, Lance D Cooley, Iain R Dixon, Kwang Lok Kim, David C Larbalestier, William S Marshall, Ulf P Trociewitz, Hubertus W Weijers, Dmytro V Abraimov, et al. The 40 T superconducting magnet project at the national high magnetic field laboratory. *IEEE Trans. Appl. Supercond.*, 30(4):4300405, 2020.
- [3] Kwangmin Kim, Kabindra Bhattarai, Kwang Lok Kim, Hongyu Bai, Iain R Dixon, Thomas A Painter, Uijong Bong, David C Larbalestier, and Seungyong Hahn. Design and performance estimation of a 20 t 46 mm no-insulation all-rebco user magnet. *IEEE Trans. Appl. Supercond.*, 30(4):4602205, 2020.
- [4] Thibault Lécrevisse, Xavier Chaud, Philippe Fazilleau, Clément Genot, and Jung-Bin Song. Metal-as-insulation HTS coils. *Supercond. Sci. Technol.*, 35(7):074004, 2022.
- [5] Matthias Durochat, Philippe Fazilleau, Xavier Chaud, and Thibault Lécrevisse. Design of all-superconducting user magnets generating more than 40 T for the SuperEMFL project. *IEEE Trans. Appl. Supercond.*, 34(5):4904305, 2024.
- [6] Superconducting magnets for the european magnet field laboratory (SuperEMFL). *H2020 Project*. www.emfl.eu/superemfl.
- [7] Satoshi Awaji, Arnaud Badel, Tatsunori Okada, Kohki Takahashi, Hiroshi Miyazaki, Satoshi Hanai, Shigeru Ioka, Shinji Fujita, Shogo Muto, Yasuhiro Iijima, et al. Robust REBCO insert coil for upgrade of 25 T cryogen-free superconducting magnet. *IEEE Trans. Appl. Supercond.*, 31(5):4300105, 2021.
- [8] T Uto, T Tosaka, T Shitaka, H Nezuka, S Hanai, H Takewa, J Inagaki, S Ioka, A Badel, Kohki Takahashi, et al. Basic design of REBCO insert coil of 33 T cryogen-free superconducting magnet. *IEEE Trans. Appl. Supercond.*, 35(5):4601405, 2025.

- [9] R. G. Sharma. *Superconductivity Basics and Applications to Magnets*. Springer, Switzerland, 2021.
- [10] Qiuliang Wang, Jianhua Liu, Jinxing Zheng, Jinggang Qin, Yanwei Ma, Qingjin Xu, Dongliang Wang, Wenge Chen, Timing Qu, Xingyi Zhang, et al. Progress of ultra-high-field superconducting magnets in China. *Supercond. Sci. Technol.*, 35(2):023001, 2021.
- [11] Kai Wang, Hao Dong, Daxing Huang, Hongjing Shang, Bowei Xie, Qi Zou, Lin Zhang, Changping Feng, Hongwei Gu, and Fazhu Ding. Advances in second-generation high-temperature superconducting tapes and their applications in high-field magnets. *Soft Sci.*, 2(3), 2022.
- [12] Y Yanagisawa, M Hamada, K Hashi, and H Maeda. Review of recent developments in ultra-high field (UHF) NMR magnets in the Asia region. *Supercond. Sci. Technol.*, 35(4):044006, 2022.
- [13] Marina Manso Jimeno, John Thomas Vaughan, and Sairam Geethanath. Superconducting magnet designs and MRI accessibility: A review. *NMR in Biomedicine*, 36(9):e4921, 2023.
- [14] B J Parkinson, K Bouloukakis, and R A Slade. A compact 3 T all HTS cryogen-free MRI system. *Supercond. Sci. Technol.*, 30(12):125009, 2017.
- [15] Steve Bates, Serge O Dumoulin, Paul JM Folkers, Elia Formisano, Rainer Goebel, Aidin Haghnejad, Rick C Helmich, Dennis Klomp, Anja G van der Kolk, Yi Li, et al. A vision of 14 T MR for fundamental and clinical science. *Magn. Reson. Mater. Phys. Biol. Med.*, 36(2):211–225, 2023.
- [16] Neil Mitchell, Jinxing Zheng, Christian Vorpahl, Valentina Corato, Charlie Sanabria, Michael Segal, Brandon Sorbom, Robert Slade, Greg Brittles, Rod Bateman, et al. Superconductors for fusion: a roadmap. *Supercond. Sci. Technol.*, 34(10):103001, 2021.
- [17] Julia Haack. Superconductivity for nuclear fusion: Past, present, and future. *Arabian Journal for Science and Engineering*, 50(5):3233–3237, 2025.
- [18] KS Haran, S Kalsi, T Arndt, H Karmaker, R Badcock, B Buckley, T Hau gan, M Izumi, D Loder, JW Bray, P Masson, and EW Stautner. High power density superconducting rotating machines-Development status and technology roadmap. *Supercond. Sci. Technol.*, 30(12):123002, 2017.
- [19] E. Pardo, F. Grilli, Y. Liu, S. Wolftaedler, and T. Reis. AC Loss Modelling in Superconducting Coils and Motors with Parallel Tapes as Conductor. *IEEE Trans. Appl. Supercond.*, 29(5):5202505, 2019.
- [20] F Grilli, T Benkel, J Hänisch, M Lao, T Reis, E Berberich, S Wolfstädter, C Schneider, P Miller, C Palmer, B Glowacki, V Clemente-Alarcon, A Smara, L Tomkow, J Teigelkötter, A Stock, J Büdel, L Jeunesse, M Staempfli, G Delautre, B Zimmermann, R van der Woude, A Perez,

S Samoilenkov, A Molodyk, E Pardo, M Kapolka, S Li, and A Dadhich. Superconducting motors for aircraft propulsion: the advanced superconducting motor experimental demonstrator project. *J. Phys. Conf. Ser.*, 1590:012051, 2020.

- [21] Fangjing Weng, Min Zhang, Tian Lan, Yawei Wang, and Weijia Yuan. Fully superconducting machine for electric aircraft propulsion: Study of AC loss for HTS stator. *Supercond. Sci. Technol.*, 33(10):104002, 2020.
- [22] Ludovic Ybanez, Alexandre Colle, Emelie Nilsson, F Berg, G Galla, M Tassisto, J Rivenc, F Kapaun, and G Steiner. ASCEND: The first step towards cryogenic electric propulsion. In *IOP Conference Series: Materials Science and Engineering*, volume 1241, page 012034. IOP Publishing, 2022.
- [23] Swarn S Kalsi, James G Storey, Justin M Brooks, Grant Lumsden, and Rodney A Badcock. Superconducting synchronous motor development for airplane applications-mechanical and electrical design of a prototype 100 kW motor. *IEEE Trans. Appl. Supercond.*, 33(5):5201806, 2023.
- [24] H. Miyazaki, M. Iwakuma, Y. Emori, H. Sasa, K. Yoshida, S. Sato, S. Miura, I. Sagara, Y. Suzuki, M. Konno, H. Hirai, and T. Izumi. Fabrication and test of a 400 kW-class fully superconducting synchronous motor using REBCO tape for an electric propulsion system. *IEEE Trans. Appl. Supercond.*, 34(5):5200506, 2024.
- [25] Elias Bögel, Marcus Collier-Wright, Kapish Aggarwal, and Manuel La Rosa Betancourt. State of the art review in superconductor-based applied-field magnetoplasmadynamic thruster technology. In *37th International Electric Propulsion Conference*, number 476. Massachusetts Institute of Technology Cambridge, 2022.
- [26] Jamal R Olatunji, Max Goddard-Winchester, Benjamin Mallett, Nicolas Strickland, and Randy Pollock. Design of a superconducting magnet for space propulsion on the international space station. *IEEE Trans. Appl. Supercond.*, 34(3):3601006, 2024.
- [27] Pawel Prajzendanc and Christian Kreischer. A review of new technologies in the design and application of wind turbine generators. *Energies*, 18(15):4082, 2025.
- [28] AB Abrahamsen, N Mijatovic, E Seiler, T Zirngibl, C Træholt, PB Nørgård, NF Pedersen, NH Andersen, and J Østergaard. Superconducting wind turbine generators. *Supercond. Sci. Technol.*, 23:034019, 2010.
- [29] Xiaowei Song, Carsten Bührer, Patrick Brutsaert, Jens Krause, Aymen Ammar, Jan Wiezoreck, Jesper Hansen, Anders V Rebsdorf, Marc Dhalle, Anne Bergen, et al. Designing and basic experimental validation of the world's first mw-class direct-drive superconducting wind turbine generator. *IEEE Trans. Energy Conversion*, 34(4):2218–2225, 2019.

- [30] Philippe Fazilleau, Simon Bagnis, Matthias Durochat, Thibault Lecrevisse, Xavier Chaud, Andrew Varney, Steven Ball, Roman Viznichenko, Andrew Twin, et al. Behavior during quenches of a 40 T magnet made of LTS and HTS parts. *IEEE Trans. Appl. Supercond.*, 34:4704805, 2024.
- [31] Anang Dadhich, Philippe Fazilleau, and Enric Pardo. A novel and fast electromagnetic and electrothermal software for quench analysis of high field magnets. *Supercond. Sci. Technol.*, 37(9):095024, 2024.
- [32] Philippe Fazilleau, Xavier Chaud, François Debray, Thibault Lecrevisse, and Jung-Bin Song. 38 mm diameter cold bore metal-as-insulation HTS insert reached 32.5 T in a background magnetic field generated by resistive magnet. *Cryogenics*, 106:103053, 2020.
- [33] E Pardo and P Fazilleau. Fast and accurate electromagnetic modeling of non-insulated and metal-insulated REBCO magnets. *Supercond. Sci. Technol.*, 37:035016, 2024.
- [34] Andries den Ouden, Chris A Wulffers, Nigel E Hussey, Gideon Laureijs, Frans JP Wijnen, Gerben FAJ Wulterkens, Mark D Bird, Iain R Dixon, and Jos AAJ Perenboom. Progress in the development of the HFML 45 T hybrid magnet. *IEEE Trans. Appl. Supercond.*, 26(4):4301807, 2016.
- [35] K Takahashi, T Okada, Y Tsuchiya, S Awaji, H Takewa, S Hanai, and S Ioka. Seven-year operation of 25 T cryogen-free superconducting magnet as a user magnet at HFLSM, IMR, Tohoku University. *IEEE Trans. Appl. Supercond.*, 34(5):4601905, 2024.
- [36] P Pugnat, R Barbier, C Berriaud, R Berthier, T Boujet, P Graffin, C Grandclément, B Hervieu, J Jousset, FP Juster, et al. 43+ T Grenoble hybrid magnet: From final assembly to commissioning of the superconducting outsert. *IEEE Trans. Appl. Supercond.*, 32(6):4300607, 2022.
- [37] E Pardo. Modeling of screening currents in coated conductor magnets containing up to 40000 turns. *Supercond. Sci. Technol.*, 29(8):085004, 2016.
- [38] Yi Li, Qiuliang Wang, and Shunzhong Chen. Quench simulation for 9.4 T MRI superconducting magnet. *Journal of Physics: Conference Series*, 507(3):032054, 2014.
- [39] Arnaud Badel, Blandine Rozier, Brahim Ramdane, Gérard Meunier, and Pascal Tixador. Modeling of 'quench' or the occurrence and propagation of dissipative zones in REBCO high temperature superconducting coils. *Supercond. Sci. Technol.*, 32(9):094001, 2019.
- [40] J Chen, M Guan, Y Tong, X Wang, and Y Zhou. Quench detection and early warning based on thermoelastic strain rate for hts tapes thermally triggered by heat spots. *Supercond. Sci. Technol.*, 36(1):015013, dec 2022.

- [41] Andrew V Gavrilin, Ernesto S Bosque, William S Marshall, Kwangmin Kim, Dylan J Kolb-Bond, Peng Xu, Iain R Dixon, Yu Suetomi, Mark D Bird, and Hongyu Bai. Comparison Between Results of Quench Simulation and Tests of a 13T REBCO Coil in a Strong Background Magnetic Field. *IEEE Transactions on Applied Superconductivity*, 34(5):1–4, 2024.
- [42] Enric Pardo, Anang Dadhich, Nikola Jerance, and Philippe Fazilleau. Screening currents increase thermal quench propagation speed in ultra-high-field REBCO magnets. *Results in Engineering*, page 108933, 2026.
- [43] Fangliang Dong, Dongkeun Park, Patricia Sadde, Juan Bascuñán, and Yukikazu Iwasa. Construction and test of the 19.6-T solid-nitrogen-cooled REBCO insert magnet for the MIT 1.3-GHz NMR system. *Supercond. Sci. Technol.*, 38(3):035016, 2025.
- [44] Xintao Zhang, Huajun Liu, Fang Liu, Liangjun Shao, Shuai Hu, Timing Qu, Jiamin Zhu, Sheng Liu, and Hongjun Ma. Design and preliminary tests of a 20-T REBCO insert coil for a 35-T all superconducting magnet. *IEEE Trans. Appl. Supercond.*, 34(3):4300405, 2023.
- [45] Liangjun Shao, Peng Song, Yufan Yan, Xintao Zhang, Mianjun Xiao, Fang Liu, Huajun Liu, and Timing Qu. Numerical analysis of screening-current induced strain in a 16 T REBCO insert within a 20 T background field. 11:115392–115402, 2023.
- [46] Philip C Michael, Dongkeun Park, Yoon Hyuck Choi, Jiho Lee, Yi Li, Juan Bascuñán, So Noguchi, Seungyong Hahn, and Yukikazu Iwasa. Assembly and test of a 3-nested-coil 800-MHz REBCO insert (H800) for the MIT 1.3 GHz LTS/HTS NMR magnet. *IEEE Trans. Appl. Supercond.*, 29(5):4300706, 2019.
- [47] Antti Stenvall, Tiina Salmi, and Erkki Härö. Introduction to stability and quench protection. In: *Numerical Modeling of Superconducting Applications*, pages 107–190, 2023. World Scientific Publishing Co Pte Ltd, https://doi.org/10.1142/9789811271441_0002.
- [48] L Bottura. A numerical model for the simulation of quench in the ITER magnets. *J. Comput. Phys.*, 125(1):26–41, 1996.
- [49] Fangliang Dong, Dongkeun Park, Wooseung Lee, Luning Hao, Zhen Huang, Juan Bascuñán, Zhijian Jin, and Yukikazu Iwasa. On fault-mode phenomenon in no-insulation superconducting magnets: A preventive approach. *Appl. Phys. Lett.*, 121(19), 2022.
- [50] Andrea Vitrano, Mariusz Wozniak, Erik Schnaubelt, Tim Mulder, Emmanuele Ravaoli, and Arjan Verweij. An open-source finite element quench simulation tool for superconducting magnets. *IEEE Trans. Appl. Supercond.*, 33(5):4702006, 2023.

- [51] E. Pardo, J. Šouc, and L. Frolek. Electromagnetic modelling of superconductors with a smooth current-voltage relation: variational principle and coils from a few turns to large magnets. *Supercond. Sci. Technol.*, 28:044003, 2015.
- [52] E. Pardo and M. Kapolka. 3D computation of non-linear eddy currents: Variational method and superconducting cubic bulk. *J. Comput. Phys.*, 344:339–363, 2017.
- [53] Enric Pardo and Anang Dadhich. Electro-thermal modelling by novel variational methods: racetrack coil in short-circuit. *IEEE Trans. Appl. Supercond.*, 33(5):5201606, 2023.
- [54] Anang Dadhich, Francesco Grilli, Louis Denis, Benoit Vanderheyden, Christophe Geuzaine, Frederic Trillaud, Dmitry Sotnikov, Tiina Salmi, Gabriel Hajiri, Kévin Berger, et al. Electromagnetic-thermal modeling of high-temperature superconducting coils with homogenized method and different formulations: a benchmark. *Supercond. Sci. Technol.*, 37(12):125006, 2024.
- [55] Carmine Senatore, Marco Bonura, and Tommaso Bagni. REBCO tapes for applications in ultra-high fields: critical current surface and scaling relations. *Supercond. Sci. Technol.*, 37(11):115013, 2024.
- [56] Clément Genot. *Numerical and experimental studies for the optimization and protection of NI-MI HTS coils*. PhD thesis, Université Grenoble Alpes, France, 2022.
- [57] Jaap Kosse, Henrique Rodrigues, Michal Duda, Thomas Michlmayr, Stephan Müller, Dmitry Sotnikov, André Brem, Stéphane Sanfilippo, and Bernhard Auchmann. Design of NI HTS solenoid for PSI positron production experiment. *Supercond. Sci. Technol.*, 38(3):035008, feb 2025.
- [58] Yeekin Tsui, Elizabeth Surrey, and Damian Hampshire. Soldered joints – an essential component of demountable high temperature superconducting fusion magnets. *Supercond. Sci. Technol.*, 29(7):075005, 2016.
- [59] Jeongmin Mun, Changhyung Lee, Kideok Sim, Changyoung Lee, Minwon Park, and Seokho Kim. Electrical characteristics of soldered metal insulation REBCO coil. *IEEE Trans. Appl. Supercond.*, 30(4):4701904, 2020.